14th International Symposium on Turbulence and Shear Flow Phenomena (TSFP14)
Heidelberg, Germany, July 28–31, 2026

EFFECT OF LOCALIZED WALL HEATING ON CROSSFLOW INSTABILITY IN A SWEPT-WING BOUNDARY LAYER

Gaia Barocco
Department of Flow Physics and Technology
Delft University of Technology
Kluyverweg 1, Delft, The Netherlands
G.Barocco@student.tudelft.nl

Yifu Chen
Department of Flow Physics and Technology
Delft University of Technology
Kluyverweg 1, Delft, The Netherlands
Y.Chen-20@tudelft.nl

Marina Barahona
Department of Flow Physics and Technology
Delft University of Technology
Kluyverweg 1, Delft, The Netherlands
M.BarahonaLopez@tudelft.nl

Jordi Casacuberta
Department of Flow Physics and Technology
Delft University of Technology
Kluyverweg 1, Delft, The Netherlands
J.CasacubertaPuig@tudelft.nl

INTRODUCTION

Electrifying aircraft propulsion is a promising route to reduce aviation's climate impact. Unlike conventional turbofans, which reject most waste heat in the exhaust stream, batteries and fuel cells produce substantial heat that must be ultimately rejected via external heat exchangers, incurring mass and pressure-drag penalties (Schlabe & Lienig, 2014). New approaches, such as Outer Mold Line cooling, use the aircraft's skin as a heat exchanger to address these constraints. While effective for heat rejection, these methods can promote laminar-turbulent transition and thus increase skin-friction drag.

A main route towards transition in subsonic swept-wing flow involves the amplification of the crossflow instability. This instability is associated with crossflow, a secondary mean flow in the boundary layer that develops in the direction orthogonal to the trajectory of the inviscid streamlines. The present study focuses on the stationary crossflow instability (S-CFI), which dominates the transition process in low-disturbance environments such as in free flight.

Previous studies on thermal effects on boundary-layer stability have primarily examined Tollmien-Schlichting (TS) waves under uniform (Kachanov et al., 1974) and localized (Dovgal et al., 1990; Masad, 1995) heating or cooling. For the S-CFI on swept wings, uniform heating acts destabilizing, while uniform cooling acts stabilizing (Ren & Kloker, 2022). However, the influence of a localized heating or cooling surface region on the evolution of S-CFI remains largely unexplored.

This article investigates how an isolated, localized heated surface region affects the stability of the stationary crossflow instability in a compressible subsonic swept-wing boundary layer. The analysis is restricted to stationary perturbation effects. Unsteady perturbations ultimately leading the laminar-turbulent transition process are discarded, since their inclusion would likely mask the main stationary mechanisms considered in the present analysis.

Laminar base flows for heated surface regions with varying chordwise location and width are computed by solving the Compressible Boundary-Layer (CBL) equations, alongside a reference, adiabatic base flow. The growth of the stationary crossflow instability on the computed base flows is evaluated using the Compressible Linear Parabolized Stability Equations (CLPSE) method. Direct Numerical Simulations (DNS) of the compressible Navier-Stokes equations are performed to scrutinize effects of perturbation amplitude on the interaction mechanisms between the S-CFI and the heated surface region. The effect of heat-induced base-flow features on the evolution of the stationary crossflow instability and the associated mechanism of production are assessed qualitatively and quantitatively.

METHODOLOGY

1 SETUP OF THE FLOW PROBLEM

The setup of the flow problem is guided by wind-tunnel experiments performed on a 45° swept flat plate in the TU Delft A-tunnel, a low-turbulence ($T_u \leq 0.05\%$) vertical wind tunnel (Barahona et al., 2026). The domain is aligned with the Cartesian coordinate system, $\mathbf{x} = [x\ y\ z]^{\mathrm{T}}$, that is oriented with respect to the swept flat plate: x is the leading-edge-orthogonal (or, chordwise) direction, y is the wall-normal direction, and z is the leading-edge-parallel (or, spanwise) direction. The effect of sweep is modelled by decomposing the inflow free-stream velocity vector into components orthogonal, u_∞, and parallel, w_∞, to the leading-edge direction. Furthermore, the chordwise evolution of the free-stream flow velocity, u_e, is prescribed, and obtained from the experiments of Barahona et al. (2026).

The velocity vector, $\mathbf{v} = [u\ v\ w]^{\mathrm{T}}$, is decomposed into a laminar unperturbed base flow, $\mathbf{v}_{\mathrm{B}}$, and a perturbation field, $\mathbf{v}'$, such that $\mathbf{v} = \mathbf{v}_{\mathrm{B}} + \mathbf{v}'$. In the PSE computations, the perturbation field is expressed as $\mathbf{v}'(x,y,z) = \tilde{\mathbf{v}}(x,y)\, \mathrm{e}^{\mathrm{i}\left(\int_{x_0}^{x} \alpha(\xi)\, \mathrm{d}\xi + \beta_0 z\right)} + \mathrm{c.c.}$, where $\beta_0 \in \mathbb{R}$, $\alpha = \alpha_r + \mathrm{i}\alpha_i$, and $\tilde{\mathbf{v}} = \tilde{\mathbf{v}}_r + \mathrm{i}\tilde{\mathbf{v}}_i$. The base flow is con-

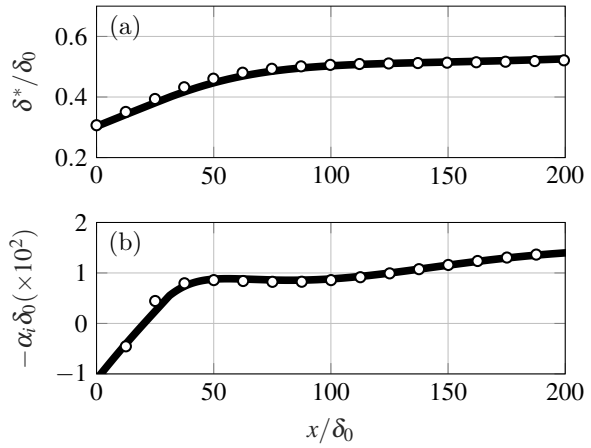

Figure 1: Cross-validation of the CBL and CLPSE (symbols) and DNS (solid) methods for (a) the displacement thickness of the base flow and (b) the S-CFI growth rate, both for adiabatic conditions.

ceived as a three-dimensional spanwise-invariant flow field. The fluid flow is assumed to be a calorically perfect gas, the effect of temperature on viscosity, $\mu = \mu(T)$, is modelled using Sutherland's law, and the Prandtl number is set to 0.71.

A laminar boundary layer is prescribed at the inflow, which is obtained as the solution of the Falkner-Skan-Cooke equation. The inflow boundary-layer thickness based on the chordwise-velocity profile, $\delta_0 = 8.01 \times 10^{-4}$ m, the chordwise free-stream velocity, $u_\infty = 10.69$ m/s, and the free-stream temperature $T_\infty = 296.7$K are chosen as reference quantities. The Reynolds number is $\mathrm{Re} = u_\infty \delta_0 / \nu_\infty = 405.81$ and the Mach number is $\mathrm{M}_\infty = u_\infty / \sqrt{\gamma R T_\infty} = 0.03$, where $\gamma = 1.4$ is the ratio of specific heats, and $R = 287$ J/(kg K) is the specific gas constant for air.

The strip is characterized by two control parameters, namely its width, denoted by Δ, and its chordwise location, defined by the x-position of the strip's centre, x_{ce}. The strip locations are $x_{ce}/\delta_0 = [236, 300, 364]$, and the strip widths are $\Delta/\delta_0 = [112, 131, 150]$.

In the strip, the chordwise evolution of the wall temperature follows a smooth square-pulse function based on a difference of sigmoids, see Figure 3 (a) for a visual representation, that peaks at $T_w = 1.5T_\infty$ in all cases considered in this work. Within the parametric space defined by x_{ce} and Δ, a baseline strip configuration is established for $x_{ce}/\delta_0 = 300$ and $\Delta/\delta_0 = 112$, hereafter referred to as the baseline strip case.

2 SETUP OF THE SIMULATIONS

The numerical simulations in this work are performed sequentially: first, the CBL equations are solved to obtain the laminar unperturbed base flow. Second, the CLPSE method is applied to the computed base flow to assess the linear evolution of the S-CFI. Additionally, DNS of the compressible Navier-Stokes equations are performed with the open-source code STREAmS to compute both the laminar unperturbed base flow and the subsequent evolution of the S-CFI in the DNS base flow. In both the CLPSE and DNS computations, the inflow velocity profile is disturbed with a crossflow instability mode obtained from a linear local stability analysis, with a prescribed spanwise wavelength of $\lambda_z = 2\pi/\beta_0 = 7$ mm.

The computational domain employed for the CBL and CLPSE simulations extends to $x/\delta_0 = 600$, virtually encompassing $5\% \leq x/c_x \leq 90\%$ of the reference experiment; here, c_x denotes the length of the reference flat plate. The effect of the strip on the non-linear evolution of the S-CFI is investigated through DNS. To this aim, two different amplitude values are assigned to the inflow crossflow instability mode, namely $A^u_{(0,1)} = 0.005u_\infty$ and $A^u_{(0,1)} = 0.02u_\infty$. Here, $(0,n)$ denotes a pertinent spanwise S-CFI mode composing the perturbation field, where $n = 1$ denotes the fundamental mode ($\beta = \beta_0$) and $n > 1$ denote the higher-order harmonic modes ($\beta > \beta_0$).

In the DNS, the grid contains $(n_x, n_y, n_z) = (3000, 220, 64)$ nodes. To constrain the growth of the S-CFI in x, periodic boundary conditions are applied at the transverse boundaries, and the domain length in z equals the spanwise wavelength of the S-CFI. A cross-validation of the CLPSE method and the DNS is shown in Figure 1 for reference, adiabatic conditions; the boundary layer displacement thickness is evaluated as $\delta^* = \int_0^\infty \left(1 - \frac{\rho u}{\rho_e u_e}\right) \mathrm{d}y$, where ρ denotes the density and ρ_e denotes the free-stream density. A cross-validation of the CLPSE and DNS methods for the baseline strip case is additionally shown in Figure 6.

The present amplitude choices ensure that the centre of the strip in the baseline strip case is located within the region of linear S-CFI growth in the low-amplitude case, and that it shifts to the region of non-linear growth in the high-amplitude case.

3 FORMULATION OF PRODUCTION

A compressible formulation of the production term of the Reynolds-Orr equation is considered in this work,

$$\mathrm{P}_{\beta_0} = -\int_V \rho_B \left(\upsilon'_{(0,1)} + \mathrm{c.c.}\right) \cdot \left[\left(\upsilon'_{(0,1)} + \mathrm{c.c.}\right) \nabla\right] \upsilon_B \, \mathrm{d}V, \tag{1}$$

see Padilla Montero & Pinna (2021) for reference. Substitution of the PSE perturbation ansatz into Equation (1) and integration over one spanwise wavelength, $2\pi/\beta_0$, yield

$$\mathrm{P}_{\beta_0} = -\frac{2\pi}{\beta_0} \int_S \rho_B \Lambda_{\beta_0} \mathrm{d}x\mathrm{d}y, \tag{2}$$

with

$$\Lambda_{\beta_0} = \left(\hat{\upsilon}_{(0,1)} + \mathrm{c.c.}\right) \cdot \left[\left(\hat{\upsilon}_{(0,1)} + \mathrm{c.c.}\right) \nabla\right] \upsilon_B, \tag{3}$$

where $\hat{\upsilon}$ encapsulates both the perturbation shape and the chordwise perturbation growth. The reader is referred to Casacuberta et al. (2022, 2024) for specific details on the present formulation of production.

RESULTS AND DISCUSSION

1 BASE-FLOW ORGANIZATION

The presence of the strip alters the organization of the incoming boundary layer. The elevated near-wall

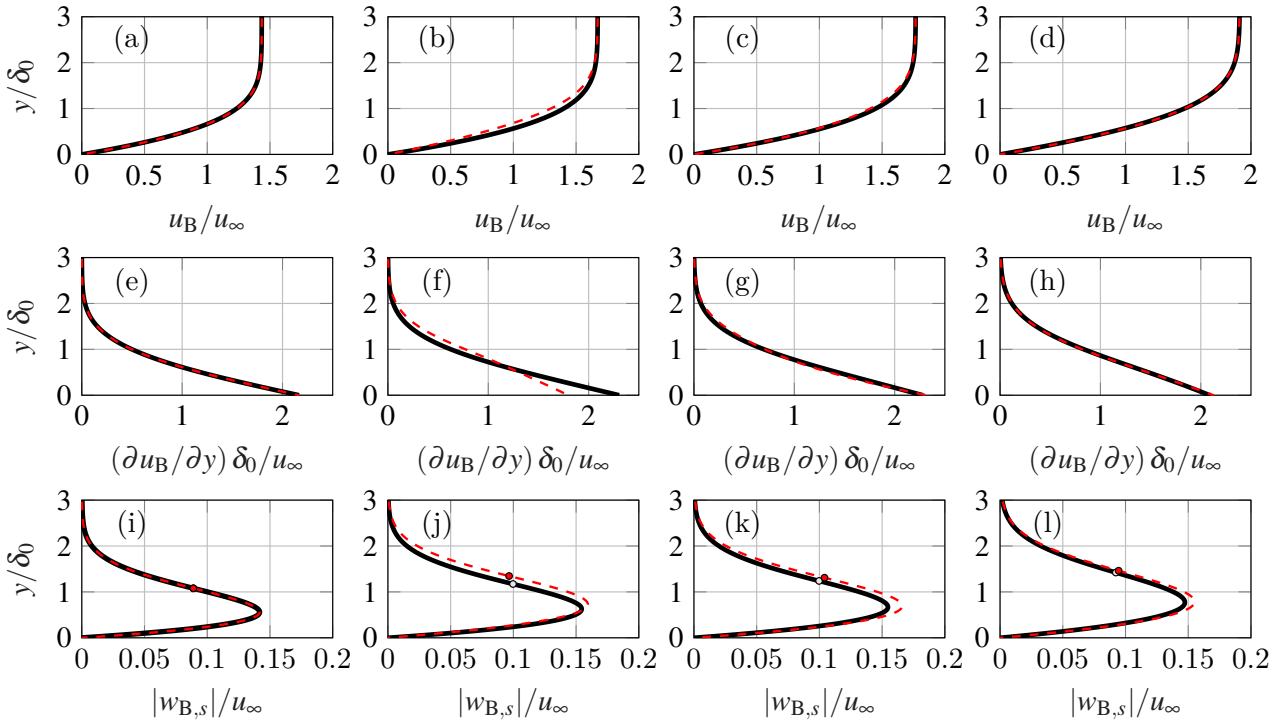

Figure 2: Chordwise velocity (a-d), wall-normal shear (e-h), and crossflow velocity (i-l) profiles in the reference, adiabatic (solid black) and the baseline strip (dashed red) cases at $x/\delta_0 = 200$ (a,e,i), 300 (b,f,j), 350 (c,g,k), 450 (d,h,l)

temperature induced by the strip increases the near-wall viscosity, thereby promoting boundary-layer thickening. This thickening remains spatially localized, i.e., it is confined to the chordwise location of the strip and its immediate downstream vicinity.

The strip also modifies the momentum redistribution across the boundary layer (Figure 2). However, both the chordwise-velocity profile, u_B, and its wall-normal shear, $\mathrm{d}u_B/\mathrm{d}y$, converge towards the reference, adiabatic conditions shortly downstream of the strip (Figure 2 (b,c,f,g)). It is noted that the base-flow organization immediately upstream of the strip is not significantly affected by its presence (Figure 2 (a,e)).

The boundary layer of swept-wing flow is three-dimensional. It exhibits an inflectional profile, the crossflow profile, $w_{B,s} = w_B\cos(\phi_s) - u_B\sin(\phi_s)$, that points in the direction orthogonal to the inviscid streamline. Here, $\phi_s = \phi_s(x)$ is the *local* angle between the inviscid streamline and the x-direction. As shown in Figure 2 (i-l), the crossflow profile exhibits greater sensitivity to the strip than the chordwise velocity profile, u_B.

Specifically, the strip enhances the peak magnitude of the crossflow velocity profile in x, $\max(|w_s|)$ (Figure 3 (c)), and shifts the crossflow inflection-point location, y_{IP}, upward (Figure 3 (b)). This modification of the crossflow velocity profile by the strip is consistent with previous studies on the effect of uniform (i.e., extended along the chordwise direction, as opposed to the present isolated strip) wall heating on swept-wing boundary-layer flow (Barahona et al., 2026).

In the case of the strip, the deviations in y_{IP} relative to reference, adiabatic conditions are mainly spatially confined to the strip and its immediate downstream vicinity (Figure 3 (b)). Contrarily, the increase in $\max(|w_s|)$ reaches its maximum near the trailing edge of the strip and recovers towards the reference, adiabatic conditions only gradually in x, over a long chordwise distance (Figure 3 (c)). Figure 3 (b,c) confirms that the aforementioned trends are qualitatively consistent among all tested strip configurations.

A plausible explanation for the increase in $\max(|w_s|)$ far downstream of the strip (Figure 3 (c)) is elaborated as follows: despite the wall temperature relaxing rapidly in x, the warmer fluid convected from the strip and away from the wall maintains a temperature higher than the reference, adiabatic case. The density is thereby reduced away from the wall, i.e., close to the y-locations where the crossflow velocity profile peaks. The resulting lower density increases the strength of the crossflow velocity profile, relative to reference, adiabatic conditions (Ren & Kloker, 2022).

2 LINEAR PERTURBATION EVOLUTION

In the present section, the CLPSE method is employed to assess the linear evolution of the S-CFI under both adiabatic and strip conditions, while non-linear perturbation effects are assessed below through DNS.

Upon introduction of the strip, the growth of the S-CFI is modified, relative to the reference, adiabatic case, both in the vicinity of the strip and further downstream of it. The effect of the strip is overall destabilizing, albeit a localized stabilization occurs near the leading edge of the strip, as shown in Figure 3 (d). Note that in this work, $-\alpha_i > 0$ and $-\alpha_i < 0$ denote perturbation growth and decay, respectively.

For completeness, Figure 4 (b) quantifies the perturbation amplification factor, $N(x) = \int_{x_0}^{x} -\alpha_i(\xi)\,\mathrm{d}\xi$, expressed relative to the adiabatic case, N_{ad}. Here, x_0 de-

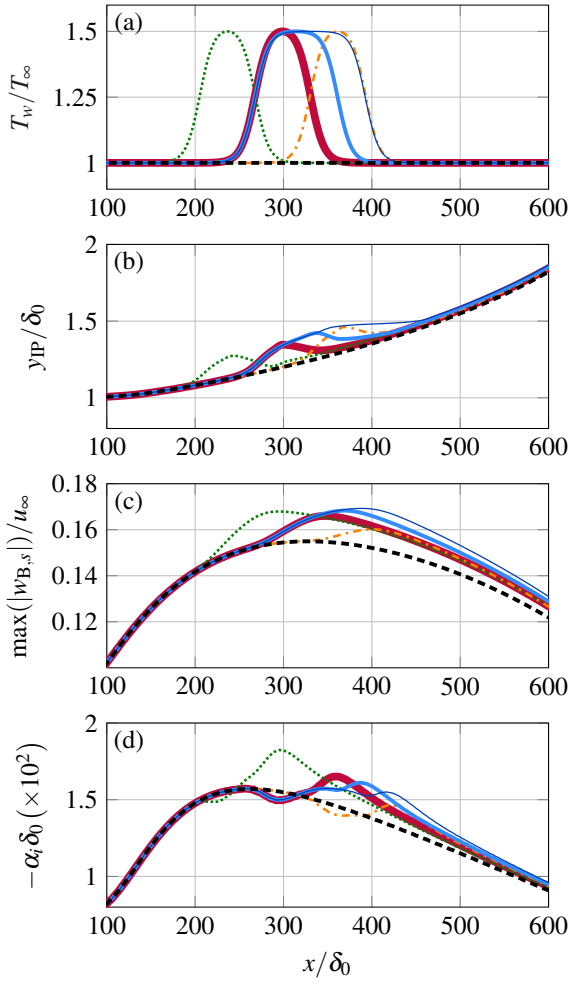

Figure 3: Chordwise evolution of the wall temperature (a), the wall-normal crossflow inflection point location (b), the strength of the crossflow velocity profile (c), and the S-CFI growth rate obtained from CLPSE (d) for the different strip cases. Lines indicate the reference, adiabatic case (dashed black), the baseline strip case (very thick solid red), and the remaining strip cases, namely for an upstream shift (dotted green), downstream shift (dash-dotted orange), and width increase (solid thick light blue and solid thin dark blue) of the strip.

notes the chordwise location of the neutral point (i.e., $\alpha_i = 0$), and ξ is a dummy variable. Figure 4 (b) confirms that the strip linearly destabilizes the pre-existing S-CFI across all cases considered. Furthermore, the largest destabilization is produced by either shifting the strip upstream (sdotted green line) or by increasing the width of the strip (see thin solid dark blue line).

The linear destabilizing influence of the strip is ascribed to two distinct growth effects: first, the pronounced destabilization of the S-CFI locally at the trailing edge of the strip. Second, further downstream, the fact that the perturbation growth rate recovers towards that of the reference, adiabatic conditions only gradually (Figure 3 (d)); the slow spatial adaptation of the perturbation growth rate yields an extended chordwise region of enhanced perturbation growth. Both these effects are qualitatively consistent across all tested strip configurations (Figure 3).

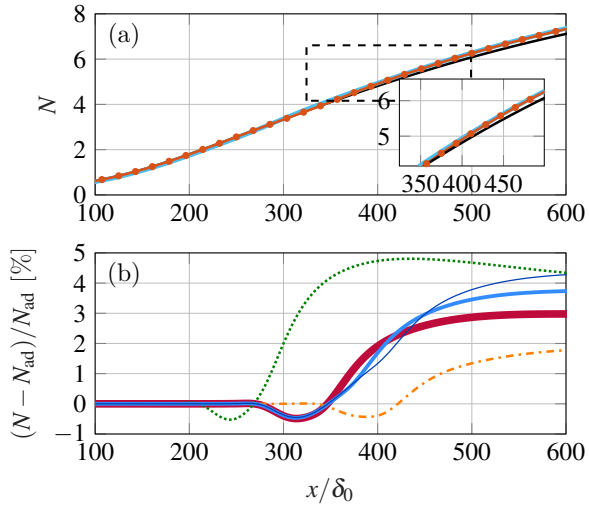

Figure 4: (a) Comparison of perturbation amplification factor, N, between the baseline strip case computed through ILPSE (solid blue) and CLPSE (solid orange with circles). The reference, adiabatic case is shown in solid black line. (b) Chordwise evolution of the perturbation amplification factor for the different strip cases obtained from CLPSE. For style, see caption in Figure 3.

The aforementioned region of enhanced perturbation growth extends beyond the chordwise location at which the main structure of the boundary layer has already recovered to that of the reference, adiabatic case. This is evidenced, for instance, by comparing Figure 3 (d) with Figure 2 (d,h) (which illustrates the chordwise velocity profile and its wall-normal shear at $x/\delta_0 = 450$), as well as by the chordwise evolution of the crossflow inflection-point location shown in Figure 3 (b).

Increasing the width of the strip increases this *perturbation adaptation length*, defined here as the chordwise distance downstream of the strip over which the perturbation growth rate recovers towards the reference, adiabatic growth rate (Figure 3 (d)).

3 MECHANISMS OF LINEAR INTERACTION BETWEEN THE CROSSFLOW INSTABILITY AND THE STRIP

3.1 The role of temperature Insight into the mechanisms underlying the modified perturbation behavior due to the strip described above is gained through a heuristic exercise: the solutions of the compressible (CLPSE) and incompressible (ILPSE) formulations of the PSE method are compared using the same base flow, i.e., obtained as the solution of the compressible boundary layer equations.

As shown in Figure 4 (a) illustrating the baseline strip case, the agreement between the CLPSE and ILPSE methods provides evidence that the destabilization of the S-CFI by the strip is not directly governed by variable thermal properties and temperature-related perturbation effects.

3.2 Perturbation production Building on the insights gained above regarding the role of temperature, the present section examines the behavior of the produc-

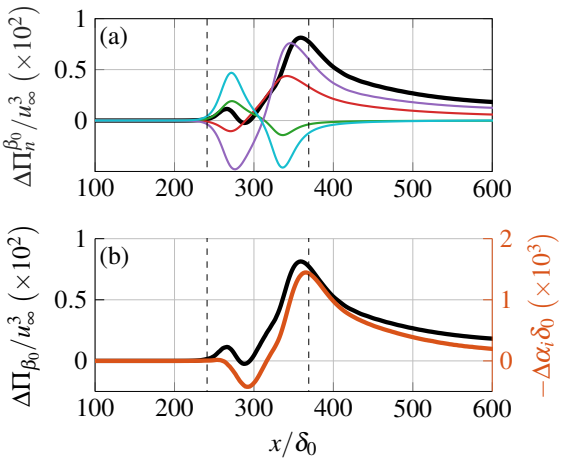

Figure 5: (a) Chordwise evolution of the production terms $\Pi_n^{\beta_0} = \int \Lambda_n^{\beta_0} \mathrm{d}y$ (Equation 3) computed from CLPSE, expressed relative to the reference, adiabatic case. (b) Chordwise evolution of *total* production (Π_{β_0}, thick black line) (Equation 3) and S-CFI growth rate (α_i, thick orange line), expressed relative to the reference, adiabatic case. Here, the *increment* operator is defined as $\Delta(\cdot) = (\cdot)_{\mathrm{strip}} - (\cdot)_{\mathrm{adiabatic}}$. In panel (a): Π_{β_0} (thick black line), $\Pi_1^{\beta_0}$ (blue line), $\Pi_2^{\beta_0}$ (purple line), $\Pi_5^{\beta_0}$ (green line), $\Pi_6^{\beta_0}$ (red line). Dashed vertical lines indicate the extent of the strip. Results are shown for the baseline strip case.

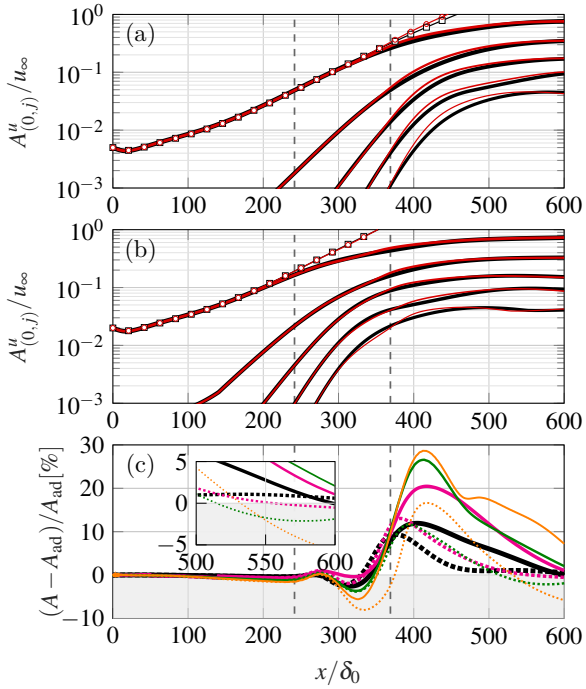

Figure 6: Chordwise evolution of the amplitude of modes j = 1-5 (thick to thin) in the reference, adiabatic case (black) and the baseline strip case (red) when the inflow S-CFI amplitude is (a) $A^u_{(0,1)}/u_\infty = 0.005$ and (b) $A^u_{(0,1)}/u_\infty = 0.02$. The CLPSE results are indicated with black squares (adiabatic case) and red circles (strip case). (c) Amplitude difference between the baseline strip and the reference, adiabatic cases for $A^u_{(0,1)}/u_\infty = 0.005$ (solid lines) and $A^u_{(0,1)}/u_\infty = 0.02$ (dotted lines). Modes j = 1-4 are shown in black, magenta, green and orange, respectively. Dashed vertical lines indicate the extent of the strip.

tion mechanism, which condenses information on the base-flow velocity gradients, in relation to the mechanisms feeding growth to the S-CFI.

Figure 5 (a) illustrates the chordwise evolution of production, i.e., $\Pi_{\beta_0} = \int \rho_B \Lambda_{\beta_0} \mathrm{d}y$ (thick black line) and the terms composing production, i.e., $\Pi_n^{\beta_0} = \int \rho_B \Lambda_n^{\beta_0} \mathrm{d}y$ (thin color lines),

$$\Lambda_1^{\beta_0} = \left(\hat{u}\hat{u}^\dagger + \mathrm{c.c.}\right)\frac{\partial u_B}{\partial x}, \quad \Lambda_2^{\beta_0} = \left(\hat{u}\hat{v}^\dagger + \mathrm{c.c.}\right)\frac{\partial u_B}{\partial y},$$
$$\Lambda_5^{\beta_0} = \left(\hat{w}\hat{u}^\dagger + \mathrm{c.c.}\right)\frac{\partial w_B}{\partial x}, \quad \Lambda_6^{\beta_0} = \left(\hat{w}\hat{v}^\dagger + \mathrm{c.c.}\right)\frac{\partial w_B}{\partial y}. \quad (4)$$

The contribution of the terms $\Pi_3^{\beta_0}$ and $\Pi_4^{\beta_0}$ is found to be negligible and thus disregarded from the analysis in the present section. More specifically, Figure 5 (a) quantifies the *increment* of the corresponding terms with respect to the reference, adiabatic case; note that here $\Delta\Pi_n^{\beta_0} = \Pi_n^{\beta_0}|_{\mathrm{strip}} - \Pi_n^{\beta_0}|_{\mathrm{adiabatic}}$.

At the strip's leading-edge region ($240 < x/\delta_0 < 305$), the terms associated with the chordwise ($\partial u_B/\partial x$) base flow velocity gradients (i.e., $\Pi_1^{\beta_0}$ and $\Pi_5^{\beta_0}$, see blue and green lines in Figure 5) exhibit a trend opposite to those associated with the wall-normal ($\partial u_B/\partial y$) base flow gradients (i.e., $\Pi_2^{\beta_0}$ and $\Pi_6^{\beta_0}$, see purple and red lines in Figure 5). That is, the former are larger than in adiabatic conditions, whereas the latter are lower than in adiabatic conditions. The opposite holds true at the strip's trailing-edge region ($305 < x/\delta_0 < 370$).

The growth of $\Pi_1^{\beta_0}$ and $\Pi_5^{\beta_0}$ at the strip's leading-edge region leads to a net increase of *total* production in this region, i.e., $\Delta\Pi_{\beta_0} > 0$ across $240 < x/\delta_0 < 305$, see thick black line in Figure 5. At the strip's trailing-edge region ($305 < x/\delta_0 < 370$), the evolution of *total* production is instead driven by the terms associated with the wall-normal base flow gradients, $\Pi_2^{\beta_0}$ and $\Pi_6^{\beta_0}$. Next to it, Figure 5 (b) shows that, in the strip case, the S-CFI growth rate and production follow a qualitatively similar evolution in x.

It is noted that the production term $\Pi_2^{\beta_0}$ (associated with $\partial u_B/\partial y$), mainly dominates the evolution of *total* production downstream of the strip (see purple line in Figure 5 (a)), while the base flow shear $\partial u_B/\partial y$ recovers towards reference, adiabatic conditions rapidly downstream of the strip (Figure 2 (e-h)).

A similar effect has been recently reported in the context of a pre-existing S-CFI interacting with a localized smooth surface protrusion in an incompressible boundary layer (Westerbeek et al., 2026). Specifically, the authors show that the smooth surface protrusion deforms the pre-existing CFI into a less unstable structure over an extended chordwise region downstream of the protrusion, despite the base flow recovering to the no-protrusion conditions shortly downstream of it. The mechanism uncovered by Westerbeek et al. (2026), which is also supported by energy-budget analyses based on production (Casacuberta et al., 2022, 2024), could

potentially support the modified growth rate of the S-CFI in the present flow case.

At the same time, it is emphasized that, unlike the flow case of Westerbeek et al. (2026), in the present work not all base flow quantities relax towards reference, adiabatic conditions rapidly in x. Specifically, Figure 3 (c) shows that the crossflow velocity profile remains enhanced in the interaction with the strip over a large chordwise distance downstream of the strip. This effect may also be linked to the slow spatial recovery of the S-CFI growth rate shown in Figure 3 (d).

4 NON-LINEAR PERTURBATION EVOLUTION

The DNS results expand the analysis by elucidating on non-linear perturbation effects in the mechanisms of interaction between the S-CFI and the strip. Both the primary S-CFI (i.e., fundamental spanwise wavelength) mode and its accompanying high-order harmonics (i.e., smaller spanwise wavelength) modes are significantly destabilized near the strip's trailing edge (Figure 6), as also reported for the primary S-CFI in the linear stability analysis. Upon comparing the two cases for different amplitude of the inflow S-CFI mode, it is also shown that the strip destabilizes the S-CFI most effectively when it is placed in the region of linear growth.

Contrary to the results from the linear stability analysis carried out through CLPSE, the results from DNS reveal that the primary S-CFI mode decays significantly further downstream of the strip through non-linear perturbation interactions. Overall, the high-order harmonic modes exhibit different growth trends downstream of the strip indicating that the mechanisms of perturbation growth and decay are, at least, a function of the initial amplitude of the S-CFI and the perturbation mode under consideration.

CONCLUSIONS

The Compressible Linear Parabolized Stability Equations (CLPSE) method is employed to investigate the effect of a localized heating surface region (strip) on the linear evolution of the stationary crossflow instability (S-CFI) in a compressible subsonic swept-wing boundary layer. Direct Numerical Simulations (DNS) of the compressible Navier-Stokes equations are performed to assess the non-linear evolution of the S-CFI in the presence of the strip. The structure of the unperturbed laminar base flow and the evolution of the S-CFI are characterized and discussed. The present analysis, restricted to stationary perturbation mechanisms, is guided by the wind-tunnel experiments of Barahona et al. (2026) and focuses on the effects of the strip both locally and downstream of it.

The strip induces a momentum redistribution across the boundary layer. Major structural features of the boundary layer, such as the chordwise velocity profile, recover rapidly towards reference, adiabatic conditions downstream of the strip. However, this is not the case for the *strength* of the crossflow velocity profile (i.e., the peak velocity in the direction orthogonal to the inviscid streamline), which is overall enhanced by the strip.

Linear stability analysis performed through the CLPSE method indicates that the strip linearly destabilizes the S-CFI across all cases considered. The largest increase in the linear amplification factor downstream of the strip is obtained for the cases in which the strip is positioned closest to the leading edge or has the largest chordwise extent. The DNS results, which account for non-linear perturbation effects, additionally reveal that the primary S-CFI mode (i.e., the fundamental spanwise wavelength) undergoes amplitude decay further downstream of the strip, eventually recovering to values comparable to those of the reference, adiabatic case.

The present results demonstrate that the linear destabilization of the S-CFI by the strip does not solely stem from the local modulation of the base flow in the vicinity of the strip, but also from the slow spatial adaptation of the perturbation growth rate toward the reference, adiabatic conditions over an extended chordwise distance downstream of the strip. The chordwise extent of this adaptation region, here termed the perturbation adaptation length, is found to increase with the chordwise extent of the strip.

Future work should further scrutinize the underlying mechanism sustaining the enhanced linear growth of the S-CFI that persists downstream of the strip. Two candidate mechanisms stand out: the production-mechanism modification reported by Westerbeek et al. (2026) for a localized surface protrusion, and the strip-induced enhancement of the crossflow velocity profile.

REFERENCES

Barahona, M., Chen, Y., Rius-Vidales, A. F. & Kotsonis, M. 2026 Impact of wall-heating on the development of crossflow instability. Exp. Therm. Fluid Sci. p. 111743.

Casacuberta, J., Hickel, S. & Kotsonis, M. 2024 Passive stabilization of crossflow instabilities by a reverse lift-up effect. Phys. Rev. Fluids 9, 043903.

Casacuberta, J., Hickel, S., Westerbeek, S. & Kotsonis, M. 2022 Direct numerical simulation of interaction between a stationary crossflow instability and forward-facing steps. J. Fluid Mech. 943, A46.

Dovgal, A., Levchenko, V. Y. & Timopeev, V. 1990 Boundary layer control by a local heating of the wall. In Laminar-Turbulent Transition: IUTAM Symposium Toulouse/France September 11–15, 1989, pp. 113–121. Springer.

Kachanov, Y. S., Koslov, V. V. & Levchenko, V. Y. 1974 Experimental study of the influence of cooling on the stability of laminar boundary layers. Izvestia Sibirskiogo Otdielenia Akademii Nauk SSSR, Seria Technicheskikh Nauk pp. 8–2.

Masad, J. A. 1995 Transition in flow over heat-transfer strips. Phys. Fluids 7 (9), 2163–2174.

Padilla Montero, I. & Pinna, F. 2021 Analysis of the instabilities induced by an isolated roughness element in a laminar high-speed boundary layer. J. Fluid Mech. 915, A90.

Ren, J. & Kloker, M. 2022 Instabilities in three-dimensional boundary-layer flows with a highly non-ideal fluid. J. Fluid Mech. 951, A9.

Schlabe, D. & Lienig, J. 2014 Model-based thermal management functions for aircraft systems.

Westerbeek, S., Casacuberta, J. & Kotsonis, M. 2026 Linear and nonlinear interactions between stationary cross-flow instabilities and a smooth surface hump. J. Fluid Mech. 1026, A43.